Progress In Electromagnetics Research B, Vol. 62, 17–28, 2015

Generic Building Blocks for Construction of Artificial Magnetic Media

Ali Kabiri[1] and Omar M. Ramahi[2, *]

Abstract—Variety of designs for artificial magnetic materials have been proposed in the literature. In most designs such as split-ring resonators, the inductive and capacitive responses of metallic inclusions are dependent since the area and perimeter of the resonators' geometry cannot be tuned independently. In this work, three generic resonators for the design of artificial magnetic materials are proposed. The resonators are called rose curve resonator, corrugated rectangular resonator, and sine oval resonator. The proposed resonators' patterns are characterized so that their areas and perimeters vary independently. Thus, the geometries are capable of satisfying any realizable combination of area and perimeter designed for an artificial magnetic material with desired properties. Numerical studies are considered showing the effectiveness of the new geometries to fulfil design specifications.

1. INTRODUCTION

In 1999, Pendry et al. [1] proposed artificial magnetic materials (AMMs) composed of electrically small metallic broken-looped resonators referred to as split-ring resonators (SRR). Since then, variety of configurations have been proposed to exhibit enhanced magnetic properties [2–4]. Fig. 1 shows a sample set of inclusions presented in the literature. These inclusions have been employed as a building block of metamaterial slabs. In addition, numerous analytical models were developed to characterize the behavior of an AMM with a specific inclusions' configuration [1, 3–5]. It has been shown that since the feature size of the inclusions in composite media and the skin depth are much smaller than the excitation wavelength, the magnetic response of such media can be interpreted in terms of the geometric parameters of the inclusions rather than electromagnetic properties of the metals [6].

Design and fabrication of AMMs with desired properties have received tremendous attention over the last decade due to their potential applications. Unique enabling features that allow for RF and microwave applications such as miniaturizing antenna size, decoupling proximal high profile antennas and enhancing solar cells efficiency made the artificial magnetic materials (AMMs) popular [7–10]. As the applications of AMMs in RF and microwave devices are growing, a fast, precise and robust design methodology for AMMs meeting specific properties is more demanding. A reverse approach to synthesize inclusions of an AMM that provides a specified permeability with minimum allowable dispersion and magnetic loss tangent within the frequency band has recently been proposed [11]. Since many design physical parameters cannot be varied widely and arbitrarily due to fabrication and design constrains, such as board metallization thickness and conductivity and electromagnetic properties of the host medium or width of the conductor's traces, the inclusions' geometry is a reliable and available variable of the AMM synthesis. It has also been shown that by varying the inclusions' geometry, all achievable effective permeability functions of AMM structures are inclusively mapped [11]. Therefore, a generic inclusion can be geometrically determined so that the AMM exhibits desired magnetic properties.

Received 5 November 2014, Accepted 17 December 2014, Scheduled 27 December 2014

* Corresponding author: Omar M. Ramahi (oramahi@uwaterloo.ca).

[1] Harvard School of Engineering and Applied Science, Harvard University, Cambridge, MA, USA. [2] Electrical and Computer Engineering Department, University of Waterloo, Waterloo, Ontario, Canada.

The design procedure proposed in [11] uses a circuit model in design of an AMM with specific properties. The algorithm iteratively approaches a certain accuracy with respect to the design parameters. In each iteration, the pair of area and perimeter of the inclusions, (s, l), is updated to achieve specific accuracy.

Note that as the size of the inclusions is electrically small, the circuit model expresses the magnetic properties of the comprised medium in terms of the perimeter and area of the inclusions [3–6]. Thus, it was assumed that inclusions having identical area and perimeter but different shape would result in very similar responses. The validity of this assumption was investigated for particular shape in [12].

This paper presents several generic geometries that can be used to realize any combination of geometrically realizable area and perimeter (s, l) pairs. A geometrically realizable (s, l) pair is referred to as a pair that satisfies Dido's inequality, i.e., $l \geq 2\sqrt{\pi s}$ [13]. Based on Dido's constraint, among all geometries with an identical surface area, the circle has a minimum perimeter; therefore, perimeter values smaller than the perimeter of the corresponding circle are not geometrically realizable.

The generic geometries introduced here can be used to fabricate feasible AMMs. Many AMM's constituents having different shapes were introduced in the literature (see Fig. 1). These inclusions merely promise to enhance specific magnetic properties such as the effective permeability [3] or miniaturization factor [4]. However, the novel generic geometries proposed in this work not only can be used to enhance magnetic properties, but also realize desired magnetic properties. Basically, the geometries can be configured to provide specific permeability with desired dispersion function over a certain frequency bandwidth with a maximum permissible magnetic loss. In fact, by properly configuring the geometries, the desired magnetic properties can be engineered within the physical limitations of AMM reported in [6, 14].

The proposed generic geometries are parametric contours with uncorrelated perimeter and area function. Each geometry is configured by tuning parameters so that the configured contour has a specified perimeter and surface area. The produced contour is considered as the inclusion's shape with defined thickness and trace width. Finally, the desired AMM is produced by periodically aligning the configured inclusions in parallel plates normal to the axis of the inclusions. The designed AMM is analytically and numerically tested, and the results are compared. Analytical results are direct extraction of the effective permeability function from circuit-based model of the designed AMM. However, the simulation results are the effective permeability extracted from the inversion of the scattering parameters. In fact, in the numerical analysis, the AMM structure is defined by applying periodic boundary conditions along the transverse plane with respect to the illuminated plane wave.

2. THE INCLUSION'S GEOMETRY

Metallic open-loop inclusions are categorized in two general geometrical patterns based on the number of loops of inclusions and the coupling scheme. The first category is inclusions with multiple elements such as double split-ring resonators (Fig. 1(a)) and double split square ring resonators (Fig. 1(b)) or single element but spiral (Figs. 1(d), (e), (f)) or helical shape. The second category divides inclusions into broadside-coupled (where the inclusions face each other, see [6]) or edge-coupled (where the inclusions are co-planar, see [6]). Fig. 2 shows an arbitrary inclusions contour in different categories.

The most common inclusions are split circular ring resonators and split square ring resonators. The area Ar and perimeter Pr of a square and a circle are related through the equations of $Pr^2 = 16Ar$ and $Pr^2 = 4\pi Ar$, respectively. Therefore, the area and perimeter of the circle and square are strongly dependent, and cannot be tuned independently of the other. Hence, the circle or square cannot be options for the geometry of the inclusions of an AMM with desired properties. Unlike circle and square, rectangle and ellipse provide independent area and perimeter relations. For rectangle or ellipse, area and perimeter can be formulated using a system of equations in terms of two sides of the rectangle or in terms of the semi-major and semi-minor axes of the ellipse.

For a given (Ar, Pr) pair describing an inclusion and considering the rectangle for the inclusion's shape, the sides d_1, d_2 of the rectangle are determined by the roots of the following quadratic equation in terms of d_i where $i = 1, 2$:

$$d_i^2 - \frac{Pr}{2} d_i + Ar = 0 \tag{1}$$

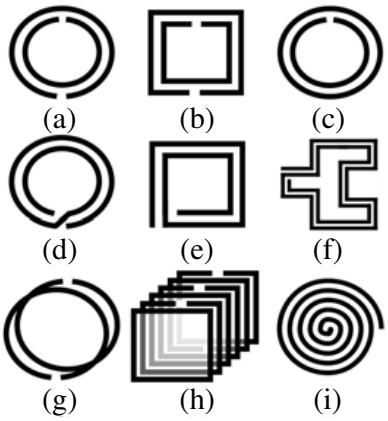

Figure 1. Different inclusions used to implement artificial magnetic materials. (a) Double Split-Ring Resonators (d-SRR), (b) Double Split Square Resonators (d-SSR), (c) Singly Split-Ring Resonator (s-SRR), (d) Two-turn (circular) Spiral Resonator (2c-SR), (e) Two-turn (rectangular) Spiral Resonator (2r-SR), (f) Hilbert-Fractal Resonator, (g) Modified Split-Ring Resonator (m-SRR), (h) Metasolenoid, (i) cross section of a Swiss Roll (SR).

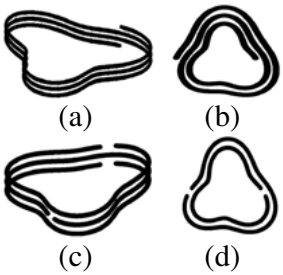

Figure 2. Different categories of inclusions. (a) Broadside-coupled 3-turn helical inclusion, (b) edge-coupled 2.5-turn spiral inclusion, (c) broadside-coupled triple split looped inclusion, (e) Edge-coupled double split looped inclusion.

When considering ellipse as the inclusion's shape, the semi-major axis r_M and semi-minor axes r_m of the ellipse are the roots of the following integral equation in terms of r_i where i stands for M, m:

$$Pr = 4r_i E\left(\sqrt{1-\left(\frac{Ar}{\pi}\right)^2 r_i^{-4}}\right) \tag{2}$$

where $E(k) = \int_0^{\frac{\pi}{2}} \sqrt{1-k^2\sin^2\theta}\; d\theta$.

Equation (1) has a real solution if $Pr^2 \geq 16Ar$. This inequality provides more restriction on the (s, l) pair calculated through the design methodology with respect to Dido's inequality. In summary, there is a set of geometrically realizable (s, l) pairs (i.e, $\{(s, l)|2\sqrt{\pi s} \leq l \leq 4\sqrt{s}\}$) which cannot be realized in a rectangular geometry.

Another constraint on the (Ar, Pr) pair is that the realized geometry has to be bounded within the unit cell area. It was shown in [6] that the s value determined through the design steps is bounded above by the inclusion's unit cell area. Therefore, $Ar \leq \delta x \cdot \delta z$, where δx and δz are the dimensions of the unit cell of an AMM. For the rectangular and elliptical shape inclusions, although the area and perimeter values are independent, the calculated sides of the rectangle or the major axes of the ellipse need to be smaller than the unit cell dimensions (for the rectangle: $d_i \leq \min(\delta x, \delta z)$ and for the ellipse: $r_M \leq \min(\delta x, \delta z)$).

These constraints define a set of restrictions on the (Ar, Pr) pair realizable by a rectangular or elliptical shape. For a rectangular shape inclusion, we have

$$\begin{cases} 0 < Ar \leq \delta x \cdot \delta z \\ 4\sqrt{Ar} < Pr \leq 2(\tau + \frac{Ar}{\tau}) \end{cases} \tag{3}$$

where $\tau = \min(\delta x, \delta z)$. Therefore, the maximum perimeter which can be obtained by rectangular inclusions is $2(\delta x + \delta z)$. Also, by considering the constraints for an elliptical shape inclusion, we have:

$$\begin{cases} 0 < Ar \leq \frac{\pi}{4}\delta x \cdot \delta z \\ 2\sqrt{\pi Ar} < Pr \leq 2\sqrt{\frac{1}{8}\pi^2\tau^2 + \frac{2Ar^2}{\tau^2}} \end{cases} \tag{4}$$

From (4), the maximum area and perimeter which can be obtained by an elliptical inclusion are 78.5% of the unit cell area and $\pi\sqrt{\frac{\delta x^2+\delta z^2}{2}}$, respectively.

3. THE AMM MODEL

In an AMM, the magnetic flux generated by the current induced on the open-loop inclusions due to the presence of an external magnetic field passes through adjacent inclusions and enhances the magnetic flux density in the medium. Therefore, the medium is magnetized. As the inclusions are periodically distributed in an AMM, at the unit cell level, the fractional area F of the unit cell occupied by the inclusion plays the key role in magnetization of the AMM. In fact, a larger fractional area receives more magnetic flux leading to a larger magnetization. Since $0 < F < 1$, for a given unit cell area $A = \delta x \cdot \delta z$, we have $0 < s < A$, where δx and δz are the dimensions of the unit cell, and s is the inclusion's area. This inequality gives an upper limit for the inclusion's area, and it is revealed that the fractional area is a real design parameters [11]. Consequently, the unit cell area can be a fixed design parameter. Note that to meet desired magnetic properties for an AMM, the perimeter of the inclusions, l, can vary as long as it does not violate the Dido's inequality.

In an AMM, as the unit cells are electrically small (i.e., smaller than the radiation wavelength), an equivalent circuit model can be proposed for inclusions and accordingly the magnetic response of an AMM. In fact, the inclusions' area and perimeter correspond to the inductance and capacitance of the equivalent circuit model, respectively. Therefore, inclusions show a resonant behavior at a frequency that the equivalent capacitance and inductance exchange equal energy back and forth. The magnetic response of an AMM can be formulated based on an equivalent circuit model and therefore, geometrical and physical parameters of the inclusions. The magnetic susceptibility of an AMM can be written in a general form of [11]:

$$\chi_m(\Omega; F, P) = \chi_0(\Omega)\left(1 + j\sqrt{\xi(\Omega)}\right)^{-1} \tag{5}$$

where Ω is the normalized frequency with respect to an inclusion's resonance frequency ($\Omega = \frac{\omega}{\omega_0}$). $\omega_0 = 2\pi f_{res}$ is the resonance frequency of an inclusion. $\chi_0(\Omega)$ and $\xi(\Omega)$ are:

$$\chi_0(\Omega) = F(s) \cdot f_1(\Omega) \tag{6}$$

$$\xi(\Omega) = \frac{P^2(sl)}{F^4(s)} \cdot f_2(\Omega) \tag{7}$$

where

$$f_2(\Omega) = \frac{f_1^2(\Omega)}{\Omega} = \frac{\Omega^3}{(1-\Omega^2)^2} \tag{8}$$

where $F = s/A$, and the physical factor P is a function of the structural and electrical properties of the inclusions.

As an example we consider a design data sheet presented in Table 1. The table summarizes a desired specification of an AMM. Although the table provides the fabrication technique parameters, it does not restrict any geometry of an AMM's inclusions. The designed steps can be summarized as follows: (1) The feasibility study, (2) Calculation of geometrical and physical factors, (3) Modification of ranges for proper tolerance, and (4) Calculation of inclusion's area and perimeter.

Following these design steps, the area and perimeter of the desired AMM's inclusions can be extracted. In fact, the AMM that satisfies specification in Table 1 is composed of inclusions with the following (s, l) pair:

$$(s, l) = (201.2\,\text{mm}^2,\ 66.66\,\text{mm}) \tag{9}$$

If considering rectangular inclusions, then by solving Equation (1), the dimensions of the inclusions are obtained as $d_1 = 25.4\,\text{mm}$ and $d_2 = 7.92\,\text{mm}$. The values for the dimensions of the inclusions are not acceptable because the larger side of the rectangle exceeds the unit cell size ($d_1 = 25.4\,\text{mm} > \delta x = 20.0\,\text{mm}$). Therefore, there are no rectangular inclusions to provide the desired magnetic properties.

Table 1. Design data sheet.

Material Specifications
Host medium: `Duroid 5880` ($\varepsilon_r = 2.2$)
Traces: `Copper` ($\sigma = 59.6\frac{S}{\mu m}$)
Fabrication Technique Parameters and Design Dimensions
Trace width: $b = 200\,\mu m$
Trace gap: $g = 800\,\mu m$
Metal thickness: $t = 35\,\mu m$
Fabrication tolerance: 0.25%
Unit cell size: $(\delta x, \delta y, \delta z) = (20.0\,mm, 800\,\mu m, 20.0\,mm)$
Design Request
Inclusion type: `Metasolenoid`
Operational frequency: $f_{op} = 600\,MHz$
Real effective permeability: $\mu_{op} \pm \delta\mu = 9.00 \pm 5.0\%$
Bandwidth: $BW \approx 2\,MHz$
Magnetic Loss Tangent (MLT): $\tan\delta < 0.050$

In the case of the elliptical inclusion, by solving Equation (2), the semi-major and semi-minor axes of the ellipse are obtained as $r_M = 15.4\,mm$ and $r_m = 4.16\,mm$. As $2r_M = 30.8\,mm > \delta x = 20.0\,mm$, thus, the ellipse cannot be confined within the unit cell.

When the calculated dimensions of the rectangular or elliptical inclusions exceed the AMM's unit cell dimensions, neither of the two geometries becomes a feasible choice for the inclusions shape, as a single inclusion cannot exceed the unit cell area.

Thus far, it has been shown that the inclusions proposed in the literature are not appropriate candidates for a generic inclusion geometry by virtue of having several geometrical limitations. Our goal is to formulate generic inclusion that can be configured to produce all geometrically realizable combination of (s, l) pairs.

Three types of parametric geometries are proposed to achieve inclusions with specific area and perimeter combination while confined to a specific unit cell. The first type has a circular base combined with a sinusoidal curve; the second type has a square base combined with a square-wave curve or corrugation on its sides; the third type is a grooved oval shape varying from an ellipse to a rectangle. Throughout, we will assume the inclusion's trace width and thickness to be negligible.

3.1. The nth Order Rose Curve

The first inclusion's geometry is a circle which is combined with a sinusoidal curve. Henceforth, the pattern is referred to as the Rose curve (see Fig. 3). This geometry has been introduced by the author in [15], and it has been comprehensively studied by Sassi et al. in [16]. The area of the produced curve is approximately equal to the area of the base circle because the area added with the sinusoidal crests is equal to the area reduced with the sinusoidal troughs. Although the area of the shape remains similar to the original circle, the desired perimeter can be adjusted by tuning the amplitude and choosing the frequency of the sinusoidal function. The fact that the area and perimeter of the Rose curve can be adjusted individually makes the Rose curve geometry a suitable candidate for the geometry of a generic inclusion. The following equation characterizes the nth order Rose curve in the polar coordinate system:

$$R_n(r_0, a) : r(\theta) = r_0 + a\cos(n\theta) \tag{10}$$

where $r(\theta)$ represents the position of the contour in the xz-plane, and angle θ sweeps the curve aside from a small slit on the contour and is measured from the x-axis; thus, $\theta \in [\frac{h}{2}, 2\pi - \frac{h}{2}]$, where h is the width of the curve's opening in radians. a is the amplitude of the sinusoidal function added to a circle

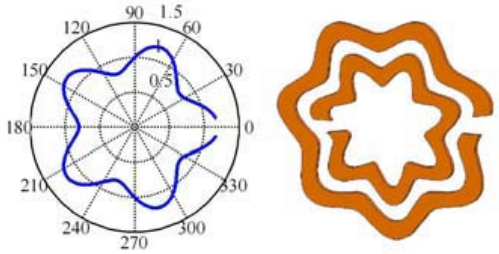

Figure 3. (a) A 5th order Rose curve with $r_0 = 1,\ a = 0.2$, (b) an edge-coupled inclusion designed using a 7th order Rose curve.

with the radius r_0. The order of the Rose curve, n, is a positive integer number and determines the number of crests and troughs along the circle's circumference. The parameters r_0 and a are calculated so that the final curve has a certain area and perimeter. Although parameter n can be chosen freely, for all geometrically realizable (s, l) pairs, there is always a minimum order for which the Rose curve can be configured to have the desired area and perimeter. In other words, by increasing the order and tuning the parameters, a Rose curve with arbitrary perimeter and confined within the unit cell can be generated. Fig. 3 shows a typical geometry for the Rose curve inclusion.

A zeroth order Rose curve and a Rose curve with $a = 0$ are simply a circle. Therefore, the Rose curve at most can cover $\frac{\pi}{4} \simeq 78.5\%$ of the unit cell area, and it cannot be used for design of inclusions, which requires area larger than 78.5% of the unit cell area (i.e., $F > 0.7854$).

The area, $Ar[R_n(r_0, a)]$, and perimeter, $Pr[R_n(r_0, a)]$, of the nth order Rose curve can be calculated using the following relations:

$$Ar[R_n] = \pi r_0^2 + \frac{\pi a^2}{2} \tag{11}$$

$$Pr[R_n] = \frac{2}{\kappa} \int_{\frac{h}{2}}^{\pi} \sqrt{1 + \eta_1 \cos n\varphi + \eta_2 \cos 2n\varphi}\ d\varphi \tag{12}$$

where

$$\begin{aligned} \kappa &= \left(2r_0^2 + a^2\left(1 + n^2\right)\right)^{-\frac{1}{2}} \\ \eta_1 &= 2r_0 a\kappa^2 \\ \eta_2 &= \kappa^2 a^2 (1 - n^2) \end{aligned}$$

Next, we design a Rose curve to achieve the design requirements expressed by (5). Table 2 presents the radius r_0 and the amplitude a of the Rose curves which is generated for different values of n ranging from 3 to 9. The last column in Table 2, parameter D gives the diameter of the circle circumscribing the Rose curve. This parameter is useful to check if the Rose curve fits within the unit cell.

Table 2. A set of candidates for rose-curved inclusions.

n	r_0 (mm)	a (mm)	D (mm)
3	7.63	3.58	22.42
4	7.80	2.70	21.00
5	7.89	2.17	20.12
6	7.95	1.81	19.60
7	8.00	1.56	19.12
8	8.02	1.36	18.72
9	8.03	1.21	18.46

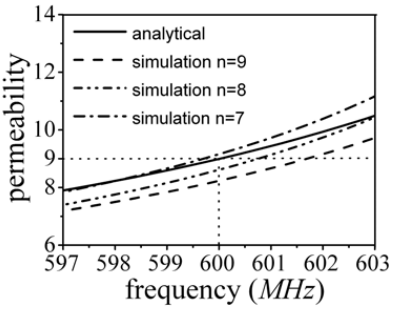

Figure 4. The dashed lines shows the simulated permeability function of the medium for $n = 7$, 8 and 9. The solid line shows the analytically calculated permeability function of the medium for $n = 7, 8$ and 9. The plots of analytical solutions cannot be distinguished because they are identical.

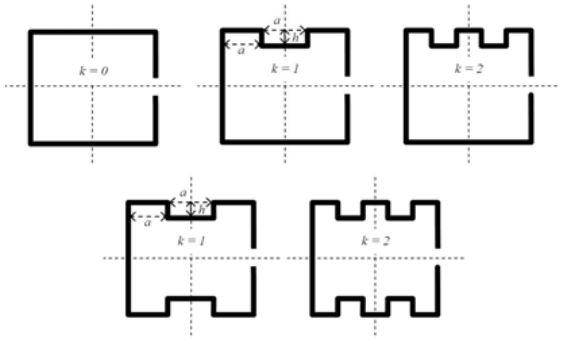

Figure 5. Corrugated Rectangular curve of the order $k = 0$, 1 and 2. The upper figures are curves with the corrugation on one side, and lower figures are curve with the corrugation on two sides.

From Table 2, for the Rose curve with $n = 3, 4$ and 5, D is larger than the size of the unit cell; therefore, the curve cannot fit within the unit cell since 20 mm $< D$. Even the 6th order Rose curve is not a good candidate for the case under consideration because if we consider the trace width of the inclusion with $n = 6$, the circumscribing circle has a diameter of $D + 0.4\,\text{mm} = 20.00\,\text{mm}$, implying the overlap of adjacent curves. Therefore, the Rose curves with $n = 7, 8$ and 9 are appropriate solutions. Rose curve with $n > 9$ presents the possibility of inter-element coupling which was not accounted for in the circuit models that are the basis for our design methodology.

Figure 4 shows the analytically and numerically calculated permeability functions of media with inclusions introduced with Rose curves of $n = 7, 8$ and 9. Throughout this work, numerical simulations were performed using the electromagnetic full wave simulator ANSYS® HFSS™. The analytical response was generated using the circuit model, and thus all the curves (for all the orders considered here) are expected to be identical because the area and perimeter of inclusions with different orders are identical. The numerical results were obtained using full-wave simulation using periodic boundary conditions to account for periodically positioned inclusions.

Note that the AMM is designed to work at the frequency of 600 MHz with 2 MHz bandwidth. Despite the fact that there is a slight shift in the resonance frequency or the maximum magnitude of the permeability function, the graphs show a robust design satisfying the design criteria. For instance, for the case of $n = 7$, the numerical simulation shows $\mu_{Re} = 9 \pm 5.6\%$ at the frequency of 599.5 MHz with 2 MHz bandwidth. The shift in frequency from the desired magnetic property requested in Table 1 is about 0.08%. The achieved MLT is 0.048 which is also within the desired range.

3.2. The *k*th Order Corrugated Rectangular Curve

The next candidate for inclusions's geometry is a square or rectangle with corrugated sides. The corrugations are a square wave added to one side or two parallel sides of the base square shape. The pattern is called Corrugated Rectangle and plotted in Fig. 5. The figure shows Corrugated Rectangular curve of the order $k = 0, 1$ and 2 over one side and two sides of a square.

The area of the final contour can be approximated as the area of the base square; however, the perimeter reaches a desired value by choosing the right order of the corrugation, i.e., the frequency of grooves and the amplitude of the added square wave. The area and perimeter of the kth order Corrugated Rectangular curves are calculated as

(i) *One-sided Corrugated Rectangle,* $C_k^1(a, h)$

$$Ar[C_k^1] = (2k+1)^2 a^2 - kah \tag{13}$$

$$Pr[C_k^1] = 4(2k+1)a + (2k)h \tag{14}$$

(ii) *Two-sided Corrugated Rectangle,* $C_k^2(a,h)$

$$Ar[C_k^2] = (2k+1)^2a^2 - 2kah \tag{15}$$

$$Pr[C_k^2] = 4(2k+1)a + 2(2k)h \tag{16}$$

Note that the length of the inclusion's slits needs to be included in the final inclusion's length. Also, $L = (2k+1)a$, the length of enclosing square of the contour, has to be smaller than the unit cell length, and $h < L$ for one side corrugation and $2h < L$ for two sides corrugation. Solving for a, we obtain:

$$a = \frac{Pr}{\gamma_1}\left(1 + \sqrt{1 + 4\gamma_1 \frac{Ar}{Pr^2}}\right) \tag{17}$$

where $\gamma_1 = 4(2k+1)(2k+3)$, and h can be obtained from (13) and (15) for the one- or two-sided Corrugated Rectangular inclusions, respectively, as:

$$h_1 = \frac{Pr}{\gamma_2}\left(1 + \sqrt{1 + 4\gamma \frac{Ar}{Pr^2}}\right) - \frac{Ar}{ka} \tag{18}$$

$$h_2 = \frac{h_1}{2} \tag{19}$$

where $\gamma_2 = \frac{2k+1}{4k(2k+3)}$.

It can be shown that for a given k, the maximum perimeter is $6(2k+1)a$. So, by increasing k, any perimeter value is achievable. As the base curve of the Corrugated Rectangular curve is a square (i.e., where $a = 0$ or $k = 0$), the minimum possible perimeter is $Pr^2 \geq 16Ar$. Thus, by calculating k, a and h, any arbitrary (s, l) pair that satisfies the square inequality can be constructed. However, in practical applications, the corrugations width cannot be very small due to coupling effects that might not be accounted for by the circuit model.

The hight and frequency of grooves in a one-sided Corrugated Rectangular curve is calculated for the area and perimeter pair given in (9). The results of the calculation for the Corrugated Rectangular curves of the first to the sixth order were summarized in Table 3. The curves are confined within the unit cell area and realizable because $h < L < \delta x$.

Table 3. A set of candidates for one-sided corrugated rectangular inclusions.

k	a (mm)	h (mm)	L (mm)
1	4.94	3.70	14.81
2	2.92	2.06	14.60
3	2.07	1.45	14.50
4	1.60	1.12	14.43
5	1.31	0.91	14.39
6	1.10	0.77	14.36
7	0.96	0.66	14.34
8	0.84	0.59	14.32

The first, second and third order Corrugated Rectangular inclusions were simulated. The simulated and analytical results are plotted in Fig. 6. The simulation of the AMM composed of the first order Corrugated Rectangular curve shows the effective permeability equal to 9 at the central frequency of 600.9 MHz. The shift from the desired magnetic property requested in Table 1 is about 0.15%. From the simulation, the frequency bandwidth for ±5% deviation from the central permeability is about 1.9 MHz, and the magnetic loss tangent is less than 0.041.

Note that for the higher order curves (6, 7 and 8), if we consider the inclusion's trace width b, the grooves walls become so close that they create unpredicted capacitive coupling which was not considered in the circuit model.

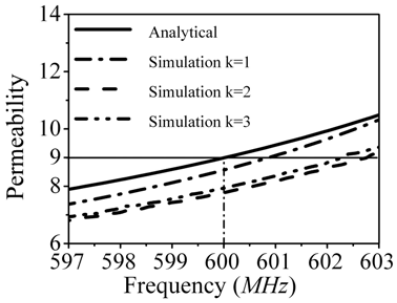

Figure 6. The dashed lines shows the simulated permeability function of the medium for $k = 1$, 2 and 3. The solid line shows the analytically calculated permeability function of the medium for $k = 1, 2$ and 3. The plots of analytical solutions cannot be distinguished because they are identical.

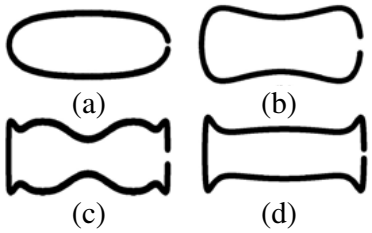

Figure 7. Samples of the Sine Oval curve, (a) $m = 0,\ \beta = 1,\ \alpha_0 = 0.5$, (b) $m = 1,\ \beta = \alpha_0 = 1,\ \alpha_1 = 2.5$, (c) $m = 3,\ \beta = 1\alpha_0 = \alpha_1 - 1 = \alpha_2 - 2 = \alpha_3 - 2.5 = 0.5$, (d) $m = 4,\ \beta = \alpha_0 = \alpha_3 = \alpha_4 = 1,\ \alpha_1 = \alpha_2 = 2.5$.

3.3. The mth Order Sine Oval Curve

The Rose curve and Corrugated Rectangular curve have limitations. The Rose curve cannot cover the whole area of the unit cell as it has a circular base, and the Corrugated Rectangular curve cannot approach the Dido's inequality [13] as it has a rectangular base. An ideal curve needs to be reconfigured to a circle for approaching Dido's inequality and to a square for covering the unit cell area. A curve that can accomplish such properties is an mth order Sine Oval curve. The curve is parameterized with θ in a Cartesian coordinate system and expressed in a vectorial form denoted by the vector $\overrightarrow{\Gamma}(x(\theta), z(\theta))$, where the components x and z are stated as

$$\begin{aligned} &S_m(\beta, \alpha_j) : \theta \to \overrightarrow{\Gamma}(x, z); \quad 0 \le j \le m \\ &\begin{cases} x(\theta) = \beta \cos(\theta) \\ z(\theta) = \alpha_0 \sin(\alpha_1 \sin(\ldots(\alpha_{m-1} \sin(\alpha_m \sin(\theta)))\ldots)) \end{cases} \end{aligned} \tag{20}$$

The parameter θ sweeps the curve in the xz-plane aside from a small slit of width h in radians; thus, $\theta \in [\frac{h}{2}, 2\pi - \frac{h}{2}]$. β and α_i are positive real numbers. A set of conditions limit the α_j parameters so that the area covered by the generated curve is simply connected. For $0 < \theta < \pi$, $z(\theta)$ should be positive in order to avoid curves with self-crossing points. For instance, considering $\theta = \pi/2$ and $m = 1$, we have $z(\pi/2) = \alpha_0 \sin(\alpha_1)$; thus, $\alpha_1 < \pi$. (The study of these conditions will not be considered here).

From (20), it can be shown that the zeroth order Sine Oval curve with $\beta = \alpha_0 = r$ is a circle with a radius of r. However, by increasing the order m and keeping $\beta = \alpha_0 = d$ and $\alpha_1 = \ldots = \alpha_m = \frac{\pi}{2}$, the curve approaches a square shape with sides equal to d. The key advantage of this parametric shape is that by configuring the parameters and the order of the curve, all realizable geometries possessing a pair of (s, l), ranging from a circle to a square, can be generated. Moreover, for a ceratin configuration, the shape provides the minimal curvature function. Therefore, the effect of unpredicted coupling due to adjacent traces will be less than previous topologies considered in this work. Fig. 7 shows sample shapes of the Sine Oval curve.

To explicitly determine the mth order Sine Oval curve, $(m + 2)$ parameters need to be calculated. We focus on two equations expressing the area and perimeter

$$Ar[S_m] = 2\int_0^{\pi} z(\theta) x_\theta(\theta) d\theta = -2\beta \int_0^{\pi} z \sin\theta d\theta \tag{21}$$

$$Pr[S_m] = 2\int_{\frac{h}{2}}^{\pi} |\overrightarrow{\Gamma}_\theta| d\theta = 2\int_{\frac{h}{2}}^{\pi} \sqrt{z_\theta^2 + \beta^2 \sin^2\theta} d\theta \tag{22}$$

where x_θ, z_θ and $\overrightarrow{\Gamma}_\theta$ are derivatives of $x(\theta)$, $x(\theta)$ and $\overrightarrow{\Gamma}(x,z)$ with respect to θ, respectively. The number of unknowns parameters exceeds the number of equations. Therefore, the number of unknowns needs to be reduced in order to solve Equations (21) and (22). We enforce the condition $\beta = \alpha_0$, $\alpha_j = \pi/2$ for $1 \leq j \leq m-1$ and $\alpha = \alpha_m$. The first condition confines the inclusions within a box with sides of β. It can be shown that the second condition makes the inclusions smoother at the edges and with a single trough. Thus, the mth order Sine Oval function reduces to

$$\begin{cases} x(\theta) = \beta\cos(\theta) \\ z(\theta) = \beta\sin(\varsigma_m(\theta)) \end{cases} \tag{23}$$

where $\varsigma_m(\theta) = \underbrace{\frac{\pi}{2}\sin(\ldots(\frac{\pi}{2}\sin(\alpha\sin(\theta)))\ldots)}_{m}$ for $m \geq 1$, and $\varsigma_0(\theta) = \theta$.

The area and perimeter of the mth order Sine Oval curve formulated in (23) are expressed as:

$$Ar[S_m] = -2\beta^2 \int_0^\pi \sin\theta\cos(\varsigma_m(\theta))d\theta \tag{24}$$

$$Pr[S_m] = 2\beta \int_{\frac{h}{2}}^\pi \left(\sin^2\theta + \alpha\left(\frac{\pi}{2}\right)^{m-1}\prod_{i=0}^{m}\cos^2(\varsigma_i(\theta))\right)^{\frac{1}{2}} d\theta \tag{25}$$

For the pair expressed in (9), the parameters α and β are calculated for $m = 1$ to 8. The results are summarized in Table 4. For the zeroth order Sine Oval curve, the curve reduces to a circle with the radius equal to β; therefore, there is no zeroth order Sine Oval curve that holds the specified area and perimeter. Fig. 8 shows simulation results in comparison with the analytical result. For the first order Sine Oval curve, the permeability is 9 at the frequency of 600.5 MHz which corresponds to about 0.08% shifts in frequency from the desired magnetic response expressed in Table 1. From the simulation, the frequency bandwidth for ±5% deviation over the central frequency of 600 MHz is about 2.0 MHz, and the magnetic loss tangent is less than 0.043.

As a summary, comparing the proposed geometries, the nth order Rose curve and kth order Corrugated Rectangular curve are easier to configure with respect to the mth order Sine Oval curve. However, the Sine Oval curve can be designed so that it provides minimal curvature function and thus less unpredicted capacitive coupling leading to better matching between the designed and desired AMM even for higher-order curves. For example, the simulation results for the design of the pair in (9) show that the Sine Oval curve provides the minimum error from the desired magnetic response.

For designing inclusions with area larger than 78.5% of the unit cell area, the Rose curve cannot be a candidate as it is basically a circular shape. Also, the Corrugated Rectangular curve cannot be a candidate for an inclusion with the area and perimeter follows the relation $l^2 < 16s$. However, the Sine Oval curve allows for design of any geometrically realizable (s, l) pair circumscribed within the unit cell area.

Table 4. A set of candidates for sine oval inclusions.

m	β (mm)	α (mm)
1	8.50	2.61
2	8.20	2.81
3	8.09	2.94
4	8.10	3.02
5	8.21	3.07
6	8.40	3.10
7	7.93	3.11
8	8.16	3.12

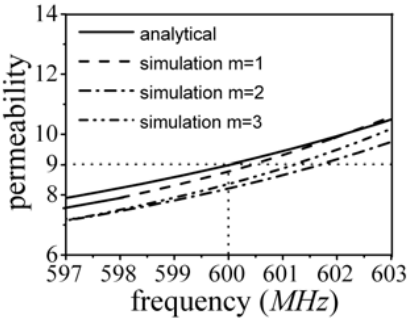

Figure 8. The dashed lines shows the simulated permeability function of the medium for $m = 1$, 2 and 3. The solid line shows the analytically calculated permeability function of the medium for $m = 1$, 2 and 3. The plots of analytical solutions cannot be distinguished because they are identical.

4. CONCLUSION

This work shows that AMM inclusions such as circular and square split-ring resonators introduced in the literature are not proper candidates for designing AMM with desired magnetic properties. This is because such inclusions have strongly interdependent area and perimeter functions. It is also shown that although the ellipse and rectangle are realized for any desired area and perimeter pair, the realized geometries can exceed the unit cell dimensions.

In order to realize AMMs with desirable magnetic properties, three sets of novel geometries for the inclusions topologies were introduced. The introduced curves are tunable to achieve any (s, l) pair calculated through the design methodology. The geometries are the nth order Rose curve, kth order Corrugated Rectangular curve and mth order Sine Oval curve. The new inclusion topologies were used to design AMM meeting specific criteria. Strong agreement was realized between the analytical results and the numerical simulations testifying to the robustness of the design methodology and flexibility and capability of the new geometries. Among the designs introduced here, the Sine Oval curve gives the best matching between the designed and desired AMMs even for higher-order curves.

REFERENCES

1. Pendry, J. B., A. J. Holden, D. J. Robbins, and W. J. Stewart, "Magnetism from conductors and enhanced nonlinear phenomena," *IEEE Transactions on Microwave Theory and Techniques*, Vol. 47, No. 11, 2075–2084, November 1999.
2. Marques, R., F. Medina, and R. Rafii-El-Idrissi, "Role of bianisotropy in negative permeability and left-handed metamaterials," *Physical Review B*, Vol. 65, No. 144440, 1–6, April 2002.
3. Maslovski, S. I., P. M. T. Ikonen, I. Kolmakov, S. A. Tretyakov, and M. Kaunisto, "Artificial magnetic materials based on the new magnetic particle: Metasolenoid," *Progress In Electromagnetics Research*, Vol. 54, No. 9, 61–81, September 2005.
4. Baena,J. D., R. Marques, F. Medina, and J. Martel, "Artificial magnetic metamaterial design by using spiral resonators," *Physical Review B — Condensed Matter and Materials Physics*, Vol. 69, No. 1, 141–145, January 2004.
5. Smith, D. R. and J. B. Pendry, "Homogenization of metamaterials by field averaging," *Journal of Optical Society America B*, Vol. 23, No. 3, 391–403, March 2006.
6. Kabiri, A., L. Yousefi, and O. M. Ramahi, "On the fundamental limitations of artificial magnetic materials," *IEEE Transanction on Antennas and Propagation*, Vol. 58, No. 7, 2345–2353, July 2010.

7. Ikonen, P. M. T., K. N. Rozanov, A. V. Osipov, P. Alitalo, and S. A. Tretyakov, "Magnetodielectric substrates in antenna miniaturization: Potential and limitations," *IEEE Transactions on Antenna and Propagation*, Vol. 54, No. 11, 391–3399, November 2006.
8. Pendry, J., "Negative refraction makes a perfect lens," *Physical Review Letters*, Vol. 85, No. 18, 3966–3969, 2000.
9. Landy, N. I., S. Sajuyigbe, J. J. Mock, D. R. Smith, and W. J. Padillal, "Perfect metamaterial absorber," *Physical Review Letters*, Vol. 100, No. 20, 207–402, May 2008.
10. Lahiri, B., A. Z. Khokhar, R. M. Delarue, S. G. McMeekin, and N. P. Johnson, "Asymmetric split ring resonators for optical sensing of organic materials," *Optics Express*, Vol. 4, No. 3, 1107–1115, January 2009.
11. Kabiri, A. and O. M. Ramahi, "Artificial magnetic materials synthesis with generic metallic broken loops," *Progress In Electromagnetics Research*, Vol. 140, 105–129, 2013.
12. Kabiri, A. and O. M. Ramahi, "Effect of curvature of metamaterial inclusions on their magnetic properties," *Proceeding of Meta'10 Second International Conference on Metamaterials, Photonic Crystals and Plasmonics*, Cairo, February 2010.
13. Forray, M. J., *Variatioal Calculus in Science and Engineering*, McGraw Hill, 1968.
14. Cummer, S. A., B.-I. Popa, and T. H. Hand, "Q-based design equations and loss limits for resonant metamaterials and experimental validation," *IEEE Transactions on Antenna and Propagation*, Vol. 56, No. 1, 127–132, January 2008.
15. Kabiri, A. and O. M. Ramahi, "nth order rose curve as a generic candidate for RF artificial magnetic material," *Applied Physics Letter*, Vol. 103, 831–834, January 2011.
16. Sassi, I., A. Kabiri, L. Talbi, and K. Hettak, "Magnetic response of n-th order rose curve resonators in the RF frequency regime," *Applied Physics Letter*, Vol. 1, No. 1, 18–25, 2012.